A model to predict deposition parameters for directed energy deposition: part I theory and modeling

Cameron Myron Knapp
Propulsion R&D, SpaceX, Hawthorne, California, USA and Department of Mechanical Engineering, University of Texas at Austin, Texas, Texas, USA
Thomas J. Lienert, Paul Burgardt and Patrick Wayne Hochanadel
Sigma Division, Los Alamos National Laboratory, Los Alamos, New Mexico, USA, and
Desiderio Kovar
Department of Mechanical Engineering, University of Texas at Austin, Texas, Texas, USA

Abstract

Purpose – Directed energy deposition (DED) with laser powder-feed is an additive manufacturing process that is used to produce metallic components by simultaneously providing a supply of energy from a laser and mass from a powder aerosol. The breadth of alloys used in DED is currently limited to a very small range as compared to wrought or cast alloys. The purpose of this paper is to develop the new alloys for DED is limited because current models to predict operational processing parameters are computationally expensive and trial-and-error based experiments are both expensive and time-consuming.

Design/methodology/approach – In this research, an agile DED model is presented to predict the geometry produced by a single layer deposit.

Findings – The utility of the model is demonstrated for type 304 L stainless steel and the significance of the predicted deposition regimes is discussed. The proposed model incorporates concepts from heat transfer, welding and laser cladding; and integrates them with experimental fits and physical models that are relevant to DED.

Originality/value – The utility of the model is demonstrated for type 304 L stainless steel and the significance of the predicted deposition regimes is discussed.

Keywords Process modeling, Directed energy deposition, Process development

Paper type Research paper

1. Introduction

Additive manufacturing allows the production of the net or near-net shape components using a layer-by-layer deposition process to yield a three-dimensional component from a computer model. The major advantage of additive manufacturing is that components may incorporate highly complex geometries produced with shorter lead times relative to conventional manufacturing processes. However, the localized fusion processing that occurs during additive manufacturing processes greatly complicates the ability to produce part geometries with high-fidelity (Knapp *et al.*, 2016). The deposit geometry as well as the microstructure and properties depend on both the elemental composition of the material and the processing parameters, suggesting that existing alloys that were optimized for conventional manufacturing processes may not be ideal for additive manufacturing and that new classes of alloys, specifically designed for additive manufacturing may be advantageous (Debroy *et al.*, 2018).

One additive manufacturing process that enables the rapid production of complex metallic parts is the LENS process (Thompson *et al.*, 2015). This process uses a combination of a laser heat source and metal aerosol powder feeder that areintegrated through a computer-numerical-controlled interface. During operation, the laser locally melts a small region on the surface as it traverses across the substrate and the powder is deposited into and captured by the molten pool; upon cooling a two-dimensional deposit results. The deposition head is repositioned to the plane of the next layer of the deposit and the process is repeated until a bulk three-dimensional component of the desired geometry is produced.

The ability to produce parts with high geometric fidelity and the desired microstructure using LENS remains challenging. Edisonian trial-and-error has traditionally been used, but this approach is costly and time-consuming and must be repeated for each new material system and specimen geometry (Heigel *et al.*, 2015). Reducing the time and expense by developing predictive models is also challenging because of several aspects

The current issue and full text archive of this journal is available on Emerald Insight at: **www.emeraldinsight.com/1355-2546.htm**

Rapid Prototyping Journal
25/6 (2019) 998–1006
 [ISSN 1355-2546]
[DOI 10.1108/RPJ-08-2018-0221]

Received 30 August 2018
Revised 1 April 2019
Accepted 30 April 2019

of the process including: rapid cooling rates (10^3-105°C/s), severe temperature gradients, the possibility of multiple phase changes and a moving heat source (Knapp *et al.*, 2016). One approach that has been successful in accurately predicting thermal histories locally within a part uses coupled computational fluid dynamics (CFD) and heat transfer models with finite element analysis simulations (Martukanitz *et al.*, 2014). Although these simulations can be very accurate, they are difficult to implement over realistic dimensions for parts produced by LENS due to the significant computational expense they require. Other analytical solutions have been proposed for portions of the LENS process (Pinkerton, 2007; Manvatkar *et al.*, 2011), but they are not integrated to a point where they are usable for a LENS framework. Thus, new approaches for models that use known or easily measurable material properties, machine parameters and implicit relevant physics are needed.

Many of the relevant constitutive equations that govern LENS have been developed for other processes, such as welding, laser cladding and heat transfer. In this paper, these existing constitutive equations are modified and integrated into a thermodynamic framework so that they can be applied to the LENS. The result is a predictive model to describe the deposit geometries resulting from LENS based on known thermophysical properties of the material, measurable machine and material parameters and controllable processing parameters. The model generally requires a numerical solution, but an analytical solution is possible by using simplifying assumptions and iterations.

1.1 Assumptions and approximations

There are a number of assumptions and approximations that are used in this model to simplify the interaction dynamics:

- *Material data*: Material properties used by this model that varies with temperature include the thermal diffusivity and density. However, the development of a model that is amenable to the analytical solution is greatly simplified if it assumed that these properties are invariant with temperature. Thus, both properties were computed by taking the average of their values at room temperature and the melting temperature (Mills, 2002). The kinematic viscosity of the material is approximated by dividing the dynamic viscosity for the dominant element in the alloy by the liquid density of the alloy; this approximation is widely used because of the limited availability of the viscosity data for molten metal alloys (Brandes, 1983). The volumetric enthalpy is calculated by a trapezoidal integration of the volumetric specific heat from the ambient temperature to the liquidus or melting temperature.
- *Processes occurring at steady-state*: The steady-state assumption implies that the effects of transients (i.e. stops, starts and changes in deposit geometries such as near corners) are short-lived (<1 s).
- *Constant absorption coefficient* η_α: In actuality, the absorptivity can vary widely. It can increase because of molten pool suppression that causes multiple scattering incidents by a single photon. Correspondingly, it can decrease for many reasons including, powder shadowing, plasma formation above the molten pool, heating of the vapor to the point that the index of refraction of the vapor can change appreciably and ejection of volatized alloying elements.

1.2 Model architecture

The overall model architecture is shown in the flow chart in Figure 1. Implementation of the model is best understood by first considering the simplest case of a single, one-dimensional deposit directly onto the substrate. The initial hypothesis is that the energy from the impinging laser is distributed across five mechanisms:

1. reflected off the substrate to the ambient environment;
2. used to melt a region of the substrate metal;
3. used to melt the captured powder;
4. used to superheat portions of the substrate and powder above the melting temperature; and
5. used to heat the substrate, up to but not beyond the melting point.

The calculation of each of these energy dissipation mechanisms forms the thermodynamic framework of the deposition model. The initiation of the model uses the concept of dilution, which is widely used in filler metal-based welding literature (Lancaster, 1999; Dupont and Marder, 1996). Dilution in the context of LENS is defined as the fraction of the melt that is not attributed to the powder added through the aerosol, multiplied by 100 per cent. For example, if 70 per cent of the mass of the solidified deposit is attributed to the powder and 30 per cent is attributed to re-melting of the substrate, then the dilution is 30 per cent. The concept of dilution in the deposition regime is used in correlating energy partitioning to mass transfer.

The model is initiated with an estimate of the dilution in an attempt to match the output dilution. The output dilution is calculated by the coupled solution of three constitutive equations in the thermodynamic framework. The initial dilution is then refined iteratively until it matches the output within a user-defined convergence criterion, at which point critical deposition parameters can be calculated; such as powder capture efficiency, melting efficiency, dilution and

Figure 1 Schematic of LENS model architecture

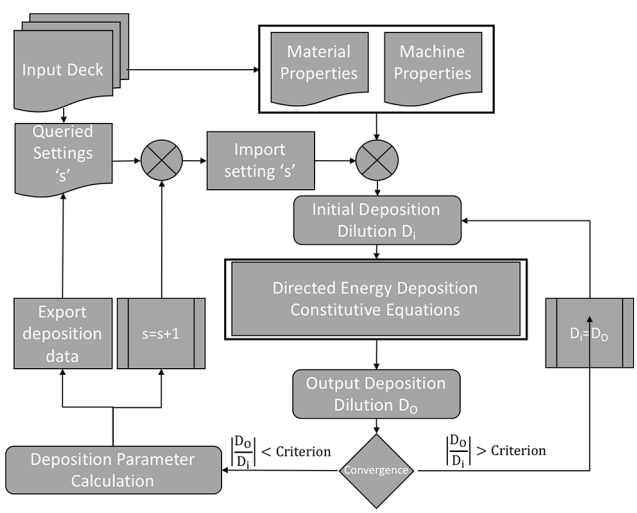

deposit width and height. Details of how each of these steps are conducted is presented in the subsequent sections.

Calibration of the machine-specific parameters

While the proposed model is intended to be universal, an accurate solution requires knowledge of machine-specific parameters that are detailed below. Both the laser optics and powder aerosol subsystems must be characterized to obtain these material- and machine-specific parameters. Both of the subsystems must then be translated into the coordinate system in which the machine operates to accurately model the system. To demonstrate the feasibility of this model, these subsystems have been characterized specifically for the Optomec LENS MR-7 used in this research. Application of this model to other machines would require characterization of these parameters for that specific system.

2.1 Optics

Traditional welding models assume that heat input occurs as a point source (Rosenthal, 1946). This assumption works functionally for welding processes where focal conditions do not change. In LENS systems, however, the laser produces a distributed heat source whose dimensions are dependent on the optics used and can change dynamically during the process as layers are added. Typically, a fiber laser has a hyperbolic profile that is focused in two dimensions to a minimum waist, which is determined by a combination of the fiber diameter, the focal length of the plano-convex lens, the off single-mode characteristics of the assembly and the wavelength of the laser. As the distance between the deposition head and the impingement of the power and laser can vary, the model of the laser profile must predict the $1/e^2$ radius at discrete orthogonal distances from the deposition head. Thus, the standard optics equation for the $1/e^2$ radius for plano-convex lenses (Seigman, 1986; CVI Optics, 2019) were modified to reproduce this laser caustic analytically in the frame of reference of the machine, while also incorporating a small measured thermal lensing effect specific to the system used. Thermal lensing occurs when optics absorb a small amount of the unfocused laser during the focusing process and heat up, resulting in geometric changes of the lens and a shift in the laser caustic. The height-dependent laser radius, $\sigma_L(z)$ is given by:

$$\sigma_L(z) = w_{0R}\left[1 + \left(\frac{(T_L P_T + z_{L0})\lambda M^2}{\pi w_{0R}^2}\right)^2\right]^{1/2} \quad (1)$$

where z is the distance between the true focus and the location of actual impingement of the laser on the substrate, W_0 is the minimum focal radius measured to be 0.135 mm, T_L is a linearization of the measured thermal lensing in the optics assembly, P_D is the power that is used and z_o = 3.5 mm and corresponds physically to the distance between the focus of the laser and substrate alignment at zero power. The ytterbium fiber-laser used in this research has a wavelength λ = 1067 nm and the non-Gaussian correction for the laser M^2, was measured to be 18.0. T_L is determined experimentally by measuring the position of the focus in the laser caustic at multiple powers P_D. The value of T_L is then computed from a linear regression of the focus shift as a function of demanded power. For the LENS system used in this research, T_L was measured to be 5.44×10^{-4} mm/W.

2.2 Energy density

Energy density is commonly used parameter for all power beam-based processes (any fusion process that uses a laser or electron beam) for convoluting processing variables and material properties correlate changes in processing or materials to results. In this research, energy density is used to assess critical process criteria that are used to predict melting efficiency, molten pool aspect ratio and the effects of laser focal condition. The proposed deposition model uses two methods for calculating an effective energy density, with each having their own distinct purpose. The first power density that was considered, P_F, was defined by Fuerschbach *et al.* [Equation (2)] and is used exclusively to determine melting efficiency (Fuerschbach and Knorovsky, 1991):

$$P_F = \frac{\eta P_T V}{E_m \alpha_L \nu} \quad (2)$$

where η_α is the absorption coefficient, P is the supplied power, V is the traverse velocity, E_m is the volumetric melting enthalpy, α_L is the thermal diffusivity and ν is the kinematic viscosity of the liquid. The Fuerschbach power density P_F, incorporates the molten properties of the metal to determine interactions in a fusion process. While the Fuerschbach model was specifically derived for arc welding, it can be used for beam process and because it is capable of incorporating implicit process variables, it provides greater utility for our model compared to the more recently developed laser welding solutions.

A second power density used was developed by Hann *et al.* (2011) [Equation (3)] and has a strong dependence on the focal condition of the laser. The Hann power density P_H is given by:

$$P_H = \frac{\eta P_T}{E_m \sqrt{\alpha_H V 2\sigma_L^3}} \quad (3)$$

where σ_L = $1/e^2$ radius of the laser at the plane of impingement. The Hann power density is used to identify deposition regimes where instabilities in molten pool formation exist, and to correlate power density and dilution to aspect ratio. Molten pool instabilities, as predicted by Hann *et al.* (2011), are unstable pool formation when $P_H < 1$ and the keyhole formation when $P_H \gtrsim 10$.

2.3 Powder feed

To calculate the amount of powder available for capture into the molten pool, the powder aerosol density must first be characterized. In powder deposition processes, no standard method is available, so a method was devised for the current work. Optomec recommends a 10 mm initial alignment offset of the deposition head to the substrate for idealized powder capture. In this paper, the 10 mm offset is referred to as the "initial alignment." Additionally, the offset from +4 to −10 mm is referred to herein as the "interaction zone." A series of experiments were performed wherein powder aerosol was

captured by a high adhesion gel (844, JT Eaton & Co., Twinsburg, OH) at approximately 1 mm interval z distances inside the interaction zone. Plan-view images were taken of the gels using a stereo microscope and were analyzed in two-dimensions. These images were then stacked to create a three-dimensional representation of the aerosol density. The geometry of the powder aerosol, laser and capturing system are shown in Figure 2(a).

The results of the characterization for the LENS MR-7 used in the current study shows that for all cross-sections, the highest powder aerosol density occurs near the centerline and decreases as the distance from the centerline increases. The radial distribution is approximately Gaussian in the queried interaction zone. Furthermore, the standard two standard deviations of this distribution can be correlated to the distance from the initial offset by a two-term polynomial, as shown in Figure 2(b). The figure shows that, for a representative powder, the two standard deviations vary from approximately 2 mm when the deposit head is 2 mm above the substrate to approximately 4 mm when the head is 10 mm above the substrate. With this characterization completed, the powder aerosol density at any discrete orthogonal distance from the deposition head within the interaction zone can be characterized by two parameters: the total powder flow rate and the distance from initial offset alignment.

2.4 Powder capture efficiency

A model to predict the powder capture efficiency during laser cladding that shares many similarities with LENS was proposed by Lin (1999). However, the laser diameter and deposition width are approximately equal in laser cladding, whereas in LENS, the laser diameter is typically much smaller than the width of the deposit. To account for the differences in the radius of the molten pool, r and the two-standard deviation radius of the power aerosol, σ_p, the equation for the capture efficiency, η_p, is modified, as shown in equation (4):

$$\eta_P = 1 - e^{-2\left(\frac{r}{\sigma_P}\right)^2} \tag{4}$$

Figure 2

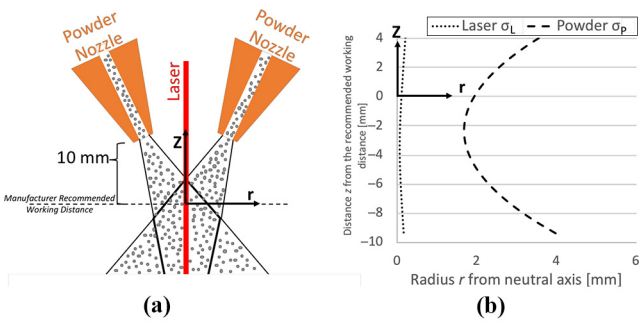

Notes: (a) Schematic of the aerosol system with interaction zone; (b) distribution of $1/e^2$ laser radius σ_L and powder aerosol standard deviation, σ_P, in the interaction zone as a function of distance from the substrate alignment, z and radius from the centerline, r

2.5 Melting efficiency

The melting efficiency, η_m, is typically used to characterize implicit physics in fusion processes such as welding (Dupont and Marder, 1996). Here we propose the use of a convoluted melting efficiency for LENS that accounts for processing conditions such as power, speed and material properties, and the effect of the significant mass introduced to the system by the powder aerosol. The injection of cold powder has the effect of decreasing the molten pool superheat by increasing the total mass in the system, and thus, increases the observed melting efficiency.

The method used by Fuerschbach and Knorovsky (1991) for calculating melting efficiency in autogenous welding is also used here to account for the heating of the substrate and is flexible in its ability to calibrate to different processes. However, an additional term is incorporated to account for the powder introduction based on experimental observations, which exhibit an inverse linear relationship between dilution and melting efficiency. The combination of these two relations yields:

$$\eta_m = A_1\, e^{\left(-B_1/P_F\right)} - (C_1 \times D) \tag{5}$$

where A_1 is the theoretical maximum melting efficiency under conduction mode conditions, B_1 is the exponential decay constant of the melting efficiency associated with P_F and C_1 is a constant that accounts for the experimentally determined inverse linear relationship between the deposition dilution, D and melting efficiency, η_M. This empirical expression is used because an analytical relationship that captures relevant physics across multiple time and length scales is not yet possible. Once these constants have been calibrated for a specific LENS machine, it is expected that they do not depend on the material system that is being used. For the machine used in this study it was determined through measurements of post-deposition metallographic cross sections that $A_1 = 0.59$, $B_1 = 27$ and $C_1 = 0.22$ for conduction-mode melting. With these constants determined for the system and interaction regimes, a closed-form relation for the melting efficiency can be defined. A plot of the σ_m vs P_F from this solution is shown in Figure 3 for 25, 50 and 75 per cent dilutions.

Notably, the theoretical maximum melting efficiency, which corresponds to A_1 is higher than the published theoretical maximums (Dupont and Marder, 1996; Fuerschbach and Knorovsky, 1991; Okada, 1977; Wells, 1952). However, this proposed value is reasonable because of two details:

1. The proposed literature is largely for autogenous power beam welding, which has a lower efficiency due to higher superheat in the molten pool. The LENS process operates with minimal superheat because of the introduction of cold metal powder into the process. The reduction of the superheat increases the apparent melting efficiency.
2. The theoretical maximum value of 59 per cent in this equation occurs when the dilution of the deposit is 0 per cent, meaning that the substrate is not melted at all. This is not physically possible for LENS as an initial molten pool must be created to enable to capture and fusion of powder. Therefore, these types of extremely low dilutions are not feasible in LENS.

Figure 3 The dependence of the melting efficiency, η_M, on the Fuerschbach power density, P_F and the dilution, D, for the Optomec LENS MR-7 used in this study

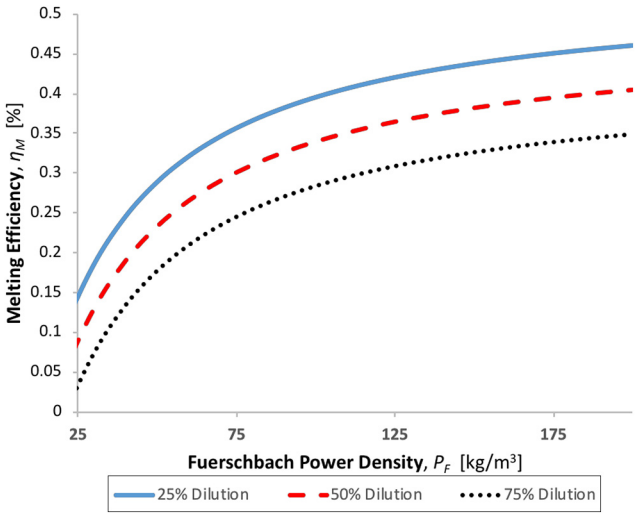

3. Governing equations

3.1 Deposition dilution

The thermodynamic balance for LENS is embodied by the dilution D, which can be determined under steady-state deposition from the respective cross-sectional areas of the deposit that are attributed to the powder A_D and the substrate A_S:

$$D = \frac{A_S}{A_S + A_D} \times 100\% \tag{6}$$

The fabricated geometry can be further linked to processing variables through the implementation of an aspect ratio relation [equation (7)], deposition rate equation [Equation (8)] and substrate melt rate equation [Equation (9)]. The implicit fluid flow equation relates the radius of the melted substrate r, to the penetration p:

$$a_C = \frac{r}{p} \tag{7}$$

The definition of the aspect ratio here is the opposite of that in conventional welding because the exposed radius of the molten pool r, is the key parameter instead of the depth. This geometric constant implicitly considers aspects of molten metal convection and surface tension that cannot be explicitly solved for in a solid-state thermodynamic solution.

The melted deposition A_D and substrate, A_S, areas can be determined by considering details of mass transfer and assuming the surface profile of the melt pool is ellipsoidal. The calculation of A_D is a geometric calculation wherein mass is related through a capture efficiency term. The ratio of the total mass flow rate, ρ, to the room temperature density ρ of the system is the total volume that is being supplied to the deposition interaction. The product of the total volume input and the capture efficiency, η_P, is the volume of deposited material. The ratio of the volume of deposited material to the traverse velocity is the deposit area created per second, A_D, as given by:

$$A_D = \frac{\eta_P \dot{m}}{V} \tag{8}$$

The area of melted substrate A_S, on the surface is assumed to be elliptical and if this area depends solely on the radius of the deposit and a_c, then the area of the melted substrate on the surface is given by:

$$A_S = \frac{\pi r^2}{2a_c} \tag{9}$$

While these basic equations define possible deposit geometries, a thermodynamic equivalency-based framework and additional physics-based mathematical models are required to create a closed form analytical expression.

3.2 Thermodynamic framework

For this iterative model, the primary criterion for convergence is dilution-informed thermodynamic equilibrium. The dilution-informed thermodynamic expression accounts for the four primary mechanisms for energy usage in the system. Although there are additional mechanisms for energy absorption, such as laser power that is absorbed into a powder that does not impinge on the molten pool, these effects sum to less than 1 per cent of the total energy for the LENS MR-7 and have therefore been ignored (Pinkerton, 2007).

The thermodynamic equivalency framework is established by balancing the amount of usable power available for the deposition against the energy dissipation mechanisms. The available power must account for the losses of laser power due to optical reflectivity, η_α and the inefficiencies of the process associated with superheating the metal beyond the required melting point. The available power is typically 5-30 per cent of the power delivered by laser, depending on the reflectivity of the material systems and the melting efficiency. The product of the volume of the deposition given by the molten metal $V(A_D + A_S)$ and the volumetric enthalpy of melting, E_M, is used to determine the power:

$$\eta_a \eta_m P_T = E_M V(A_D + A_S) \tag{10}$$

Assuming that both the powder capture efficiency, η_P and melting efficiency, η_M, are constant, a closed form solution is possible. This assumption is not strictly correct, however, and limits the useful ranges that the model can be applied. To obtain an accurate solution over a broader range of deposition parameters, the previously elaborated mathematical models for powder introduction, melting efficiency and energy partitioning are required.

3.3 Implicit molten Pool convection

Thermodynamic models do not account for material motion, such as that which occurs due to convection in the molten pool. To implicitly capture molten pool convection with restrictive boundary conditions, computationally expensive multiphase CFD must be performed. In the interest of creating an efficient model, data from experiments were instead used to generate an empirical relationship between the melted substrate aspect

ratio, a_C, the product of the Hann power density, P_H and the dilution, D:

$$a_c = E_1(P_H D)^{-2/3} \tag{11}$$

The value of E_1 must be experimentally determined by measuring the aspect ratio of the molten substrate, A_S. Experiments were used to determine the effects of the product of the P_H and the measured D on the aspect ratio, a_c, of the molten substrate, A_S area. These relations were fit with an equation that could be solved analytically with a material-specific constant E_1. As an example, the dependences of aspect ratio, a_c, on the product of P_H and D determined using this approach are shown in Figure 4 for 304 L stainless steel.

E_1 accounts for the convolution of effects that are specific to a particular material, such as the explicit molten pool convection, surface tension effects and elemental volatility that influence molten pool turbulence. It may be possible to formulate a closed form solution to this aspect ratio calculation that does not require an empirical constant; however, the required characterizations of fluid dynamics, phase changes and time constants are beyond of the scope of this model.

4. Model implementation

4.1 Model derivation

The predictive model is derived by balancing the total energy inputs against the total energy dissipated in LENS, each of which has been as described previously. This summation yields equation (12):

$$\eta_a P\left(A_1\ e^{(-B_1/P_F)} - (C_1 D_I)\right) = E_M\left[m\left(1 - e^{-2\left(\frac{r}{\sigma_P}\right)^2}\right) + \frac{\pi r^2 V}{2\left(E_1(P_H D_I)^{-2/3}\right)}\right] \tag{12}$$

Initially, D_I is assumed to be 0.5 and equation (12) is then solved for the radius of the deposit, r, which is used to calculate a final dilution, D_F in equation (13):

Figure 4 The dependence of the aspect ratio a_c, on the Hann power density, P_H and the deposition dilution, D

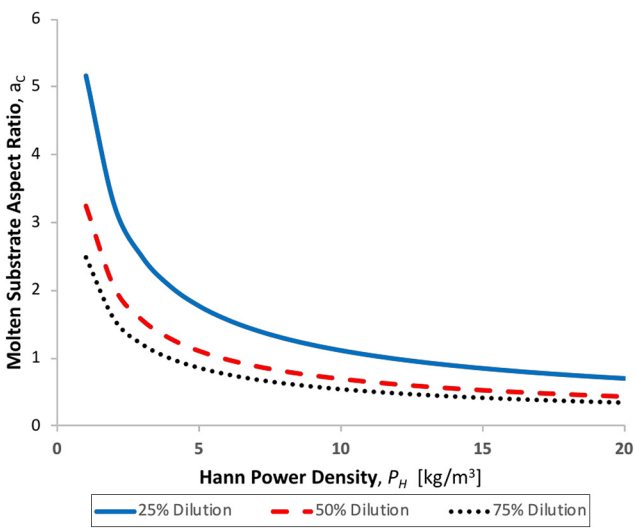

$$D_F = \frac{\frac{\pi r^2 V}{2\left(E_1(P_H D_I)^{-2/3}\right)}}{m\left(1 - e^{-2\left(\frac{r}{\sigma_P}\right)^2}\right) + \frac{\pi r^2 V}{2\left(E_1(P_H D_I)^{-2/3}\right)}} \tag{13}$$

Upon calculating D_F a single iteration is considered completed and D_I is then set to equal the new D_F. The second iteration solves equations (12) and (13) again with the new D_I and corresponding new D_F. This convergence loop repeats until D_F converges with D_I, within a user-defined convergence criterion, at which point the solution is in thermodynamic and physical equilibrium. Here, we assume a convergence criterion where D_I and D_F are within 0.5 per cent of each other.

4.2 Example application

We consider 304 L stainless steel as an example of how the model is applied to make predictions across the processing range for the LENS MR-7 used in this research. The material properties used are shown in Table I. Material properties are sourced from the literature and the ambient temperature, powder cloud two standard deviation, σ_P and implicit molten pool convection constant, E_1, are measured.

To visualize how the key deposition variables influence resultant deposition characteristics, a sensitivity analysis was performed. The deposition processing variables included laser power, P_L, traverse velocity, V, mass flow rate, $\dot{m}$ and the defocus setting. These variables were systematically varied across the entire processing range while holding the other three variables constant at a selected average processing value. The assumed average values of the processing variables were as follows: defocus = 3.175 mm, $\dot{m} = 20$ g/min, $V = 0.011$ m/s and $P_L = 700$ W. The predicted deposition characteristics including the powder capture efficiency, melting efficiency and dilution are plotted on the left axis in Figures 5(a)-(d) and the deposition width and height are plotted on the right axis in Figures 5(a)-(d) as a function of the four primary deposition variables. The deposition width is calculated by doubling the radius calculated during the convergence of equations (12) and (13). The height of the deposit is calculated volumetrically assuming an elliptical deposit using equation (14):

$$h = \frac{2\dot{m}\eta_P}{\pi r \rho V} \tag{14}$$

An increase in power, P_L, [Figure 5(a)] increases the size of the melt pool and the superheat, allowing more powder to be captured and a greater fraction of the fusion zone, therefore,

Table I Selected properties of 304 L stainless steel used in the proposed deposition model

Property	Value	Units
Absorption Coefficient, η_α	0.4	–
Density @ ½T_M, ρ (Mills, 2002)	7.69	g/cc
Volumetric Melting Enthalpy, E_M(Mills, 2002)	8.55	J/mm^3
Thermal Diffusivity @ T_M, α_T (Mills, 2002)	5.56×10^{-6}	m^2/s
Thermal Diffusivity @ ½T_M α_H (Mills, 2002)	5.36×10^{-6}	m^2/s
Kinematic Viscosity of Liquid, ν (Brandes, 1983)	0.88	mm^2/s
Implicit Convection Constant, E_1	2.05	–
Powder Cloud St. Dev, σ_P	1.94	mm

derives from the powder. Thus, increasing P_L increases all relevant deposition characteristics. An increase in laser defocus [Figure 5(b)] increases the laser spot size, resulting in a smaller superheat, a larger molten pool, and thus, a larger area to capture powder. As a result, increasing the defocus increases both the powder capture and melting efficiencies and decreases the dilution. The result is an increase in the both width and height of the deposit. An increase in traverse velocity V [Figure 5(c)] has the effect of decreasing superheat, which increases the melting efficiency. However, this does not necessarily increase the size of the molten pool as the energy can simply be used more efficiently. Additionally, the increase in traverse velocity decreases the time that the powder aerosol source is over any individual coordinate. Both of these assertions are supported by the fact that deposit width is not affected by traverse velocity, but deposit height is strongly affected. The competing effects of laser radius and time-over-coordinate explain why the powder capture efficiency is not strongly affected by the traverse velocity and can actually decrease at higher velocities. Finally, the influence of the mass flow rate, $\dot{m}$, is considered in Figure 5(d). This plot shows that increasing $\dot{m}$ increases the melting efficiency by decreasing deposition superheat through the absorption of more powder. This plot shows, however, that the additional powder does not result in an appreciable change in deposit width. Conversely, it strongly affects a positive change in the deposition height. Additionally, the decrease in dilution results in an increase in the deposition rate. However, the melt pool can only absorb a finite amount of powder, and therefore, there is no increase in powder capture efficiency associated with the increase in mass flow rate.

This sensitivity analysis is useful in visualizing and conceptualizing how changes in deposition variables can affect the efficiencies and dilution of the deposition itself. It also demonstrates the non-intuitive nature of the complex relationships between the processing parameters that justify the need for such a model.

4.3 Model limitations and uncertainties

Potential limitations in the model's ability to predict experiments can be attributed primarily to two sources, namely: the melting efficiency regression in equation (10) and the molten substrate aspect ratio regression in equation (11). The uncertainty in the empirically-derived melting efficiency is directly related to the fit of the experimental data. The fit is performed to data consisting of only the typical conduction-mode melting regime, which results in a regression that does not accurately predict the effects on non-conduction mode interactions. This means that the melting efficiency fit cannot predict behavior for departures from expected physics such as high Peclet number convective flow associated with elemental volatility or chemical interactions (Rai *et al.*, 2007), slight molten pool depressions that increase laser absorptivity of the liquid metal and the formation of vapor keyholes wherein the laser absorptivity can approach 100 per cent. At high energy densities (typically $P_H \gtrsim 10\,\mathrm{kg/m^3}$), then a transition to the vapor keyhole mode is likely and the model should not be applied. However, the actual transition to keyhole mode melting may occur below $10\,\mathrm{kg/m^3}$ depending on material system properties such as elemental volatilities, surface tension effects and/or chemical interactions.

Figure 5 Trends and sensitivity of the powder capture efficiency, η_P, the melting efficiency, η_M, dilution D, deposition width and deposition height to the processing variables that are typically controlled in LENS: velocity V, power P, mass flow rate $\dot{m}$ and laser defocus

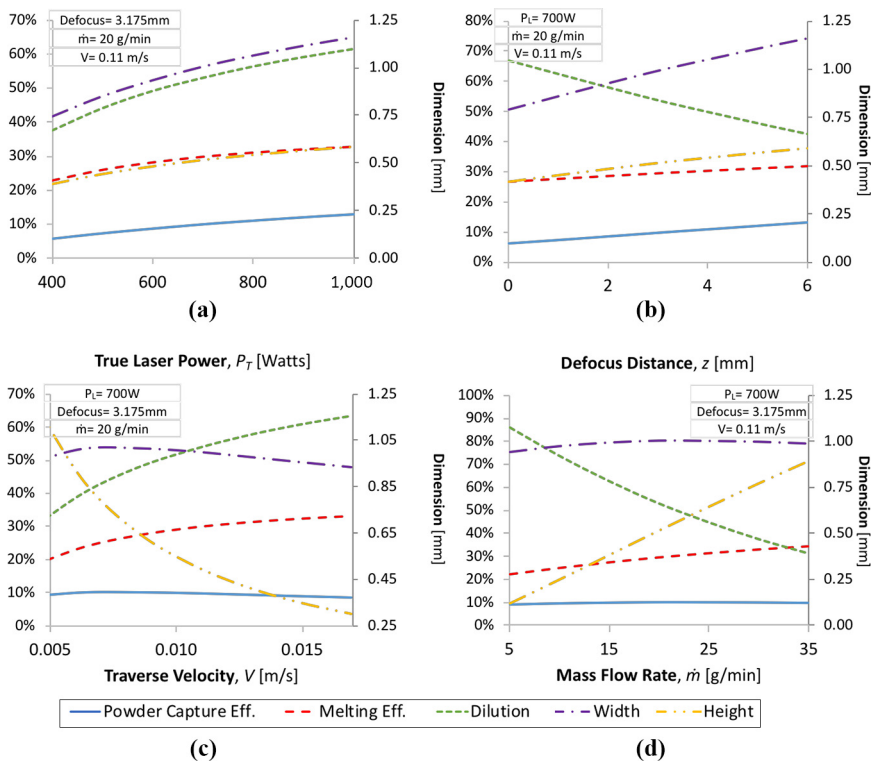

The second source of potential error is the implicit fluid flow calculation that leads to equation (11). This equation accounts for the aspect ratio of the melted substrate, which directly affects the powder capture and dilution convergence calculations. The molten substrate area aspect ratio depends on the product of the dilution and the Hann power density. This relation implicitly accounts for boundary conditions and slight changes in molten pool dynamics associated with power density, and thus, if the fit is performed over the range of processing parameters that the model will be applied, this error may be small. However, it does not account for significant molten pool effects such as vapor keyhole initiation, elemental effects on surface tension and viscosity, and changes in fluid flow convection and molten pool associated with volatilization of alloying elements and errors will be much larger if these effects are significant. These potential sources of errors suggest a range where the model can be applied successfully, which, in turn, allows operators to determine a processing window that will result in useful depositions. Generally, the model is intended to operate in the conduction melting range only ($1 < P_H < 10$); however, these limits may expand or contract based on material system specifics that are not or cannot be accounted for in the proposed model.

To determine the useful range for the model, a range of $1 < P_H < 20$ was assumed and the uncertainty in the melting efficiency and molten substrate aspect ratio were computed by taking the multiplying partial derivatives of the fitting constants in equations (3) and (11). A vector sum of the uncertainty of each constant is taken and the uncertainty of a_c and η_M result. The results are presented in Figure 6, which shows that the uncertainty in the melting efficiency ranges from 2.0-4.5 per cent at low values of P_F, depending on the dilution. The uncertainty in η_M increases before plateauing at 3.5-5.5 per cent when $P_F > 30$ kg/m^3. The uncertainty in a_c ranges from 3.0-7.0 per cent at low values of P_H and decreases until it plateaus at less than 1.0 per cent for $P_H > 10$ kg/m^3.

The total uncertainty in the model was then computed through a vector sum of the uncertainty in the aspect ratio, a_C and melting efficiency, η_M. The total uncertainty is plotted in Figure 7 versus the Hann power density P_H. This plot shows that the total uncertainty for the model is $\sim\pm4.5$ per cent, assuming $1 < P_H < 20$ and a typical 50 per cent dilution and can be as low as 3 per cent at low dilutions or as high as 8 per cent at high dilutions.

The primary limitation of the proposed model is its inability to predict performance in high power density regimes where optical interactions change to induce variable melting modes. However, at these elevated power densities, vapor keyholes become extremely likely and the associated keyhole porosity suggests this is not a practical regime for LENS processing. Ideally, a user would want to deposit as fast as possible without introducing a vapor keyhole, and thus, this model is useful for prediction of performance in conduction mode. Ultimately, this model provides LENS users the ability to predict trends and ultimate performance with reasonable accuracy without significant computational or time expenditure, allowing for the accelerated development of materials for LENS.

5. Conclusions

A physics-based model is presented that allows users to predict the deposition rate and geometry for directed energy deposition. Constitutive equations that have been developed for other processes such as, welding, laser cladding and heat transfer are modified and integrated into a thermodynamic framework, so that they can be applied to LENS. An analytical

Figure 6 Uncertainty of the regression for (a) melting efficiency as a function of the Fuerschbach power density, PF (b) the molten substrate aspect ratio fit to aC as a function of the Hann power density, PH, for varying deposition dilutions

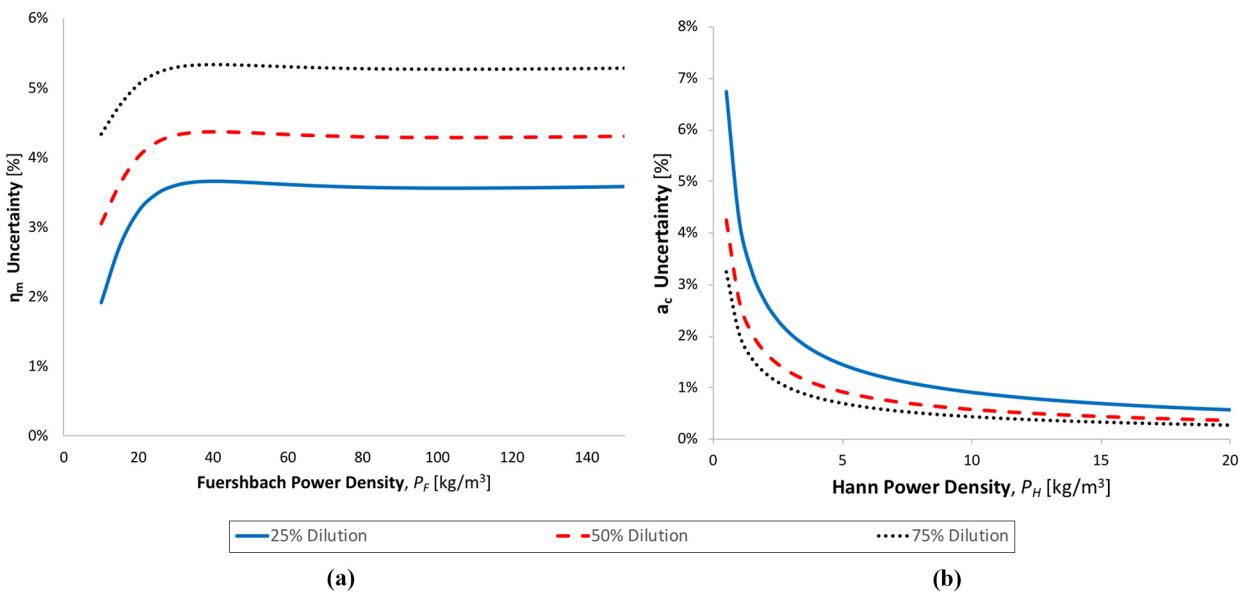

Notes: (a) Melting efficiency as a function of the Fuerschbach power density, P_F; (b) the molten substrate aspect ratio fit to a_C as a function of the Hann power density, P_H, for varying deposition dilutions

Figure 7 Total model uncertainty calculated for 304 L material system across the processing space of the LENS system used

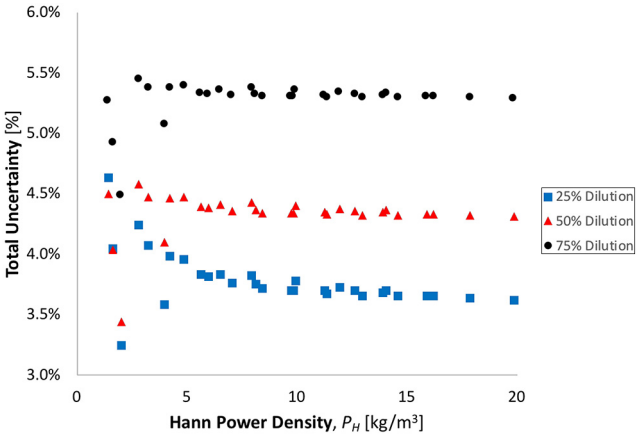

solution to the model is possible with some assumptions and calibration of the LENS system. The utility of the model is demonstrated with 304 L and a LENS MR-7 system. Predictions of the powder capture efficiency, melting efficiency, dilution and deposit dimensions are presented for a range of typical processing parameters. An error analysis suggests that the total uncertainty in the model is between 3.5-5.5 per cent, for a processing window where $1 < P_H < 20$. The predictions show how the proposed model can be used to reduce the experimental processing window that must be investigated when new materials are considered for LENS.

References

Brandes, E.A. (1983), *Smithells Metals Reference Book*, Butterworth and Co., London,

CVI Optics (2019), All things Photonic, Vol. 2, Voisins Le Bretonneaux.

Debroy, T., Wei, H.L., Mukherjee, T., Elmer, J.W., Milewski, J.O., Beese, A.M., Wilson-Heid, A., De, A. and Zhang, W. (2018), "Additive manufacturing of metallic components - process, structure, and properties", *Progress in Materials Science*, Vol. 92, pp. 112-224.

Dupont, J.N. and Marder, A.R. (1996), "Dilution in single pass arc welds", *Metallurgical and Materials Transactions B*, Vol. 27B, pp. 481-489.

Fuerschbach, P.W. and Knorovsky, G.A. (1991), "A study of melting efficiency in plasma arc and gas tungsten arc welding", *Welding Journal*, Vol. 70 No. 11, pp. 287-297.

Hann, D.B., Iammi, J. and Folkes, J. (2011), "A simple methodology for predicting Laser-Weld properties from material and laser parameters", *Journal of Applied Physics*, Vol. 44.

Heigel, J.C., Michaleris, P. and Reutzel, E.W. (2015), "Thermo-mechanical model development and validation of directed energy deposition additive manufacturing of Ti–6Al–4V", *Additive Manufacturing*, Vol. 5, pp. 9-19.

Knapp, C.M., Lienert, T.J., Kovar, D. and Carpenter, J.S. (2016), "In situ monitoring of directed energy deposition", *Conference Proceedings of MS&T 2016, Salt Lake City*,

Lancaster, J.F. (1999), *Metallurgy of Welding*, Woodhead Printing,

Lin, J. (1999), "A simple model of powder catchment in Co-Axial laser cladding", *Optics and Laser Technology*, Vol. 31 No. 3, pp. 233-238.

Manvatkar, V.D., Gokhale, A.A., Jagan Reddy, G., Venkataramana, A. and De, A. (2011), "Estimation of melt Pool dimensions, thermal cycle, and hardness distribution in the Laser-Engineered net shaping process of austenitic stainless steel", *Metallurgical and Materials Transactions A*, Vol. 42 No. 13, pp. 4080-4087.

Martukanitz, R., Michaleris, P., Palmer, T., Debroy, T., Lui, Z.-K., Otis, R., Heo, T.W. and Chen, L.-Q. (2014), "Toward an integrated computational system for describing the additive manufacturing process for metallic materials", *Additive Manufacturing*, Vol. 1-4, pp. 52-63.

Mills, K.C. (2002), *Recommended Values of Thermophysical Properties for Selected Commercial Alloys*, Woodhead Publishing

Okada, A. (1977), "Applications of melting efficiency and its problems", *Journal of the Japan Welding Society*, Vol. 46 No. 2, pp. 53-61.

Pinkerton, A.J. (2007), "An analytical model of beam attenuation and powder heating during coaxial laser direct metal deposition", *Journal of Physics D: Applied Physics*, Vol. 40 No. 23.

Rai, R., Elmer, J.W., Palmer, T.A. and Debroy, T. (2007), "Heat transfer and fluid flow during keyhole mode laser welding of tantalum, Ti-6Al-4V, 304L stainless steel, and vanadium", *Journal of Physics D: Applied Physics*, Vol. 40 No. 18, pp. 5753-5766.

Rosenthal, D. (1946), "The theory of moving sources of heat and its application to metal treatments", *Transactions of ASME*, Vol. 43 No. 11, pp. 849-866.

Seigman, A. (1986), *Lasers*, University Science Books, Mill Valley.

Thompson, S.M., Bian, L., Shamsaei, N. and Yadollahi, A. (2015), "An overview of direct laser deposition for additive manufacturing; part 1: transport phenomena, modeling and diagnostics", *Additive Manufacturing*, Vol. 8, pp. 36-62.

Wells, A.A. (1952), "Heat flow in welding", *Welding Journal*, Vol. 31 No. 5, pp. 263-267.

Corresponding author

Cameron Myron Knapp can be contacted at: cameron.knapp@spacex.com